Structure and Mechanical Properties of Giant Lipid (DMPC) Vesicle Bilayers from 20 °C below to 10 °C above the Liquid Crystal–Crystalline Phase Transition at 24 °C†

D. Needham‡,§ and E. Evans*,‡,∥

Departments of Pathology and Physics, University of British Columbia, Vancouver, British Columbia, Canada V6T 1W5

Received November 24, 1987; Revised Manuscript Received April 29, 1988

ABSTRACT: We have used micromechanical tests to measure the thermoelastic properties of the liquid and gel phases of dimyristoylphosphatidylcholine (DMPC). We have found that the rippled $P_{\beta'}$ phase is only formed when a vesicle is cooled to temperatures below the main acyl chain crystallization transition, T_c, under *zero* or *very low membrane tension*. We also found that the $P_{\beta'}$ surface ripple or superlattice can be pulled flat under high membrane tension into a planar structure. For a ripple structure formed by acyl chains perpendicular to the projected plane, the projected area change that results from a flattening process is a direct measure of the molecular crystal angle. As such, the crystal angle was found to increase from about 24° just below T_c to about 33° below the pretransition. It was also observed that the $P_{\beta'}$ superlattice did not form when annealed $L_{\beta'}$ phase vesicles were heated from 5 °C to T_c; likewise, ripples did not form when the membrane was held under large tension during freezing from the L_α phase. Each of these three procedures could be used to create a metastable planar structure which we have termed $L^*_{\beta'}$ since it is lamellar and plane-crystalline with acyl chains tilted to the bilayer plane. However, we show that this structure is not as condensed as the $L_{\beta'}$ phase below 10 °C. On the basis of observed changes in vesicle projected area at the main transition and comparison of the elastic area compressibility moduli measured for each of the structures (L_α, $L^*_{\beta'}$, and $L_{\beta'}$), the $P_{\beta'}$ phase is shown to be a soft crystalline solid that possesses some degree of chain disorder and slight liquidlike character. Below the pretransition temperature, bilayers exhibited a much lower compressibility indicative of further condensation to a more solid crystalline phase. At intermediate temperatures for the $P_{\beta'}$ phase, we observed that the rippled surface behaved in a weakly elastic manner at low membrane tensions. On the basis of this observation, we have developed a mechanical model for the rippled phase that represents the material as a pleated surface where extensional deformations of the projected plane are derived from bending deformations of the surface facets (analogous to a "corrugated spring"). This model predicts that the ripple surface elastic modulus is proportional to the bilayer bending or curvature elastic modulus and inversely proportional to the square of the ripple amplitude. The model correlates very well with the observed mechanical behavior of the $P_{\beta'}$ phase surface and yields a value for the bilayer bending modulus of 3×10^{-12} erg.

In a previous paper (Evans & Kwok, 1982) thermoelastic properties were determined for dimyristoylphosphatidylcholine (DMPC) bilayer vesicles at, and above, the main acyl chain crystallization temperature (24 °C). The projected area change at the transition was found to be consistent with X-ray diffraction measurements for the relative area change between the L_α and $L_{\beta'}$ phases (Janiak et al., 1979); i.e., the results indicated an absence of the rippled $P_{\beta'}$ phase. Recently, we have used similar micromechanical tests to extend this work and to characterize more fully the low-temperature gel phases, $P_{\beta'}$ and $L_{\beta'}$, of DMPC.

The liquid and gel phases of phospholipids, and phosphatidylcholines (PC's) in particular, have received much attention from a wide range of experimental perspectives since the early work of Chapman et al. (1967). Two enthalpic peaks, associated with the pretransition and main transition, were identified (Chapman et al., 1967), and the X-ray studies of Luzzati and Husson (1962) and Tardieu et al. (1973) described the structure of a variety of lipid and water phases above and below the main transition. The liquid L_α phase is disordered, with extensive rotational motion of the head groups and also about individual C–C bonds in the acyl chain; here, the molecule as a whole exhibits rotational and lateral diffusion. At some characteristic temperature T_c, the liquid phase makes a transition to a more ordered gel phase as a result of cooperative freezing of the hydrocarbon chains (Nagle, 1980). The transition is accompanied by a dramatic loss of lateral diffusion (Cullis, 1976) and restriction of a variety of bond motions (Marsh, 1980; Casal & Mantsch, 1984; Wong, 1984; Davis, 1983). An intermediate hexagonal $P_{\beta'}$ phase was identified (Rand et al., 1975; Janiak et al., 1975) between the more closely packed $L_{\beta'}$ and the disordered L_α phases. The $P_{\beta'}$ phase has been shown to form a periodic surface ripple (superlattice) which exists for all saturated PC's at water contents greater than about 20% in a temperature range just below T_c (Janiak et al., 1976). Several competing effects are likely to determine the structure in the gel phase, e.g., condensation of the acyl chains, packing constraints of the head groups, and interaction

† This work was supported by the Medical Research Council of Canada through Grant MT 7477. D.N. is grateful to NATO/SERC for a postdoctoral fellowship award.

* Address correspondence to this author at the Department of Academic Pathology, 2211 Wesbrook Mall, University of British Columbia, Vancouver, BC, Canada V6T 1W5.

‡ Department of Pathology.

§ Present address: Department of Mechanical Engineering and Materials Science, Duke University, Durham, NC 27706.

∥ Department of Physics.

0006-2960/88/0427-8261$01.50/0

at the water–hydrocarbon interface.

Although the gel phases are considerably more condensed than the liquid phase, the $P_{\beta'}$ and to a lesser extent the $L_{\beta'}$ phase have been shown in several studies to possess some liquidlike character. The crystal does not completely "freeze" until below a further subtransition to the L_c phase (Chen et al., 1980; Ruocco & Shipley, 1982). The primary X-ray peak profiles for DPPC show the $P_{\beta'}$ phase to contain about 35% and the $L_{\beta'}$ phase about 15% liquidlike chain conformations (Brady & Fein, 1977). Both Raman (Pink et al., 1980; Snyder et al., 1982; Vogel & Jahnig, 1981) and ^2H NMR (Davis, 1979; MacKay, 1981) studies present a picture of the gel phase as being one that is still characterized by some chain disorder. For DMPC, Raman spectra show that the average number of gauche bonds per chain changes from 7.1 to 1.1 at the main transition (Pink et al., 1980; Snyder et al., 1982; Levin & Bush, 1981) with a further reduction at the pretransition. Other Raman studies indicate that the chain interactions increase only slightly in the temperature range of the $P_{\beta'}$ phase but show a large increase as the temperature is reduced below the pretransition into the $L_{\beta'}$ phase (Wong, 1984). Even so, just below the pretransition for DPPC, the ^2H and ^1H NMR spectra are not those expected for an all-trans conformation (Davis, 1979; MacKay, 1981)—there still exists a gradient in chain flexibility. By infrared spectroscopy, the chains are observed to be predominately all-trans (Cameron et al., 1980) whereas in neutron diffraction (Büldt et al., 1979a,b) and X-ray studies (Janiak et al., 1976), the chains appear to be in a completely all-trans configuration for the $L_{\beta'}$ phase.

X-ray diffraction studies have shown that the chains are tilted (angled) to the bilayer plane for both the $P_{\beta'}$ and $L_{\beta'}$ phases. Because of the rippled surface superlattice for the $P_{\beta'}$ phase, it might be assumed that the chains are more or less lined up normal to the projected plane of the surface. However, the orientation of chains relative to the projected plane in the $P_{\beta'}$-phase domain is not well established. Rand et al. (1975) regarded the pretransition as the change from tilted to perpendicular with respect to the projected plane of the bilayer. Janiak et al. (1979, 1976), on the other hand, stated that the angle of the acyl chains to the projected plane is about 60° in the $P_{\beta'}$ phase. Most recently, Stamatoff et al. (1982) showed that for the rippled bilayer, the chains are normal to the projected plane. If the chains are normal to the projected plane for the $P_{\beta'}$ phase, the change in projected area between the liquid L_α phase and the $P_{\beta'}$ phase provides a direct measure of chain condensation. Likewise, the change in projected area between the rippled $P_{\beta'}$ phase and the planar $L_{\beta'}$ phase yields the intrinsic crystal angle of chain tilt with respect to the crystal surface. Also, the rippled structure has been directly observed in several electron microscopic studies, which identify the various phases from the characteristic texture of their freeze–etched images (Luna & McConnell, 1977; Krebecek et al., 1979). On the basis of geometric models for the ripple superlattice [e.g., sawtooth (Sackmann, 1983), symmetric (Stamatoff et al., 1982; Krebecek et al., 1979), sinusoidal (Janiak et al., 1976), folded (Larsson, 1977)], X-ray and SEM studies have been analyzed to yield dimensions for the ripple architecture. For example, the wavelength and peak-to-peak amplitude have been found to be 160 and 50 Å (Stamatoff et al., 1982) or 205 and 80 Å (Krebecek et al., 1979) for DPPC and DMPC, respectively.

In our experiments, we have used micropipet aspiration of giant bilayer vesicles as a sensitive differential area transducer (Evans & Waugh, 1977; Kwok & Evans, 1981). Because of either kinetic restrictions to filtration of water from the vesicle interior or the osmotic activity of solutes in the aqueous media, vesicle volumes remain essentially constant over the course of an experiment; thus, change in aspirated length of the vesicle inside the pipet provides a direct measure of membrane area change in response to either temperature or suction pressure changes. With this method, we have examined bilayer compressibility, thermal expansivity, and relative area changes over the range of temperatures from 5 to 35 °C which characterizes the lipid structures from $L_{\beta'}$ and $P_{\beta'}$ gel phases to the L_α liquid phase. From the direct area and mechanical measurements, we have developed a structural model of the rippled phase that embodies the intrinsic properties of single microcrystalline domains.

Experimental Procedures

Preparation of large phospholipid vesicles followed a procedure introduced by Reeves and Dowben (1969) that was modified to provide a higher yield of unilamellar structures. With their method, lipid is first dried from chloroform–methanol onto glass and then rehydrated; this approach produces mainly multilamellar and nonvesicular structures. Centrifugation must be used to separate out any suitable vesicles from this type of suspension (Reeves & Dowben, 1969; Mueller et al., 1983). By observing the rehydration process directly under the microscope, we found that unilamellar vesicles were best produced from flat thin lamellae on a substrate surface. Since chloroform–methanol has an appreciable contact angle with glass, the evaporation of solvent mainly leaves thick layers or mounds of lipid on the substrate (glass) surface. To circumvent this problem, we found that a roughened Teflon disk could be used as a substrate on which to dry the lipid film. The circular Teflon disk was roughened with emery paper to form tiny grooves oriented in one direction. The disk was thoroughly cleaned by washing in detergent, tap water, distilled water, and chloroform. It was preheated in an oven to about 40 °C prior to application of the lipid solution: 50 μL of 10 mg/mL DMPC (Avanti Polar Lipids Inc., Birmingham, Alabama) in chloroform–methanol (2:1). The solution was added to the warm disk with a syringe needle and was quickly spread over the entire surface. The solvent evaporated immediately to leave the small amount of lipid as a thin film over the whole surface. The film of lipid was then evacuated overnight to remove the last traces of solvent. In order to reliably produce vesicles from neutral lipid preparations, we found that rehydration must be carried out at temperatures above the acyl chain crystallization transition *with* nonelectrolytes or at very low ionic strength. First, the teflon disk and lipid film (in a loosely Parafilm sealed beaker) were prehydrated at 40 °C for 30 min with water-saturated argon. This allowed the closely stacked lamellae to swell and hydrate as much as possible prior to the addition of bulk water. Final hydration of the lipid was accomplished by addition of distilled water at 30–35 °C; the beaker was left covered in the oven to allow the lipid to hydrate undisturbed. As hydration progresses, large lipid tubes float off the lamellae surface and eventually pinch off into tethered "strings" of vesicles which form a "cloud" in the suspension. Vesicles were harvested by gentle pipet aspiration of the "cloud" into a 1-mL Eppendorf tube followed by dilution with warm, 35 °C, water. The amount of dilution was chosen to provide a workable concentration of vesicles that was low enough not to degrade the optical image seen through the microscope. The vesicle suspension was then injected into a temperature controlled (±0.1 °C) microchamber mounted on the microscope stage. [Note: Vesicles must be selected with care to avoid invisible microtubular attachments to other vesicles. Movement by any other

vesicle(s) in the vicinity when a vesicle is aspirated demonstrates direct connection to other vesicles via submicroscopic tethers. Many of these tethers are broken when the vesicle suspension is initially aspirated for subsequent dilution; most of the remaining tethers can be broken when vesicles are frozen at temperatures below T_c.]

For the experiments to be reported in this paper, vesicles were made and suspended in distilled water. Even though these vesicles lacked inside osmotic activity, which acts to keep the volume constant in opposition to filtration forces, vesicle volumes remained essentially constant over the duration of pipet aspiration experiments because the filtration pressures were low and because the vesicle membrane permeability was low, especially for frozen lipid. For the range of suction pressures used in these experiments (up to ~0.03 atm), we have observed that it takes 1 h or more to filter out 1% of the volume. Thus, for experiments over a period of a few minutes, the aqueous contents of the vesicles were kinetically trapped. Since vesicles were formed initially as spheres with trapped-volume contents, only increases in vesicle area could occur without buildup of large membrane stresses (Kwok & Evans, 1981). On the other hand, condensation of the surface by freezing the lipid caused rapid buildup of thermoelastic stress in the membrane that was followed by vesicle rupture. Excess volume was violently expelled from the contracting vesicle before the membrane defect could reseal. In many instances, this defect in the frozen membrane remained open and aspiration caused the vesicle to crumple and fold as it entered into the pipet. Ruptured vesicles were easily resealed by briefly raising the temperature to T_c and cooling again before the unsupported excess area could pinch off and form a tethered daughter vesicle. With this procedure, sufficient excess area (over that of a sphere of equivalent volume) was created so that the membrane could be cooled through the main transition to low temperatures without buildup of membrane stresses. Because of the requirement for large excess area to permit cycling through the lipid phase transition without sphering, there was a restricted range of aspect ratio (R_o/R_p) for the radius of the outer spherical portion of the vesicle to the radius of the micropipet. If a vesicle was too large, excessively large tongue lengths were formed which would neck in and pinch off at low suction pressures. On the other hand, if a vesicle was too small, the outer spherical portion of the vesicle became too small and would not support large suction pressures.

Tests Performed. Four micropipet experiments were devised to examine the effect of stress on vesicle area versus temperature behavior:

(i) Vesicles, which had been preformed with sufficient excess area to pass unstressed through the main transition, were aspirated by micropipet and cooled from the L_α state above 24 °C through the main transition (at a rate of 10 °C/min) under zero or very low membrane tensions (0.16 dyn/cm). The temperature was lowered (at 1 °C/min) to the pretransition then cooled further (at 0.1 °C/min) to about 5 °C. Subsequently, this temperature course was reversed to take the vesicle back to the L_α state above T_c.

(ii) Similarly, vesicles were cooled from the L_α state through T_c to low temperatures under moderate tension levels (fixed at 0.2 or 2.0 dyn/cm), cooled to 5 °C, and subsequently reheated to the L_α state.

(iii) Vesicles, which had again been preformed with sufficient excess area to pass unstressed through the transition as in (i), were cooled to 4 °C and kept refrigerated at that temperature for several days. Then, these vesicles were subjected to the tension test (0–6 dyn/cm) at 8 °C. Finally, the vesicles were heated to the L_α state above T_c under very low membrane tension.

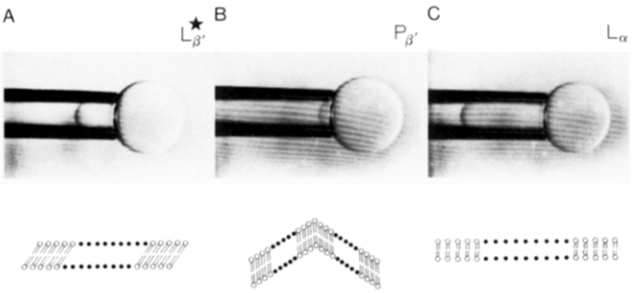

FIGURE 1: Three photographs of the same vesicle in the three states of condensation corresponding to the phases $L^*_{\beta'}$, $P_{\beta'}$, and L_α [(A), (B), and (C), respectively]. The rippled vesicle in (B) with acyl chains perpendicular to the projected plane is aspirated and heated through T_c, giving a 22% area change (C). It is then cooled back through the transition under stress to form the planar $L^*_{\beta'}$ structure, with chains tilted to the projected plane and, concomitantly, larger projected area (A).

(iv) The same preformed vesicles were cooled from the L_α state through T_c to specific temperatures (20, 16, and 12.5 °C) under zero or very low tensions. Then, at constant temperature, the vesicles were stressed by pipet suction pressure to produce a range of tensions (0–6 dyn/cm) up to the level for vesicle rupture.

In each experiment, vesicle area changes were derived from aspiration lengths in the micropipet as either a function of membrane tension at constant temperature or a function of temperature at constant membrane tension (Kwok & Evans, 1981).

RESULTS

Figure 1 presents videomicrographs of a particular vesicle at three conditions: (C) above T_c at 25 °C in the L_α liquid state; (A) below T_c at 16 °C in the $L^*_{\beta'}$ frozen state where the rippled surface superlattice was not allowed to form because of large membrane stress; (B) below T_c at 16 °C in the stress-free $P_{\beta'}$ state produced by vesicle rupture and resealing at low membrane stress. Vesicles were initially formed in the $P_{\beta'}$ state, illustrated by Figure 1B. The L_α state was reached simply by heating vesicles through the main transition. The $L^*_{\beta'}$ phase was produced by subsequent cooling of vesicles from the L_α state under moderate to large membrane stress *or* by application of membrane stress to vesicles formed initially as the stress-free state shown in Figure 1B *or* by annealing vesicles under refrigeration at 4 °C for several days and heating to temperatures between T_p and T_c.

Figure 2 shows the projected area measured for single DMPC vesicles in water as a function of temperature between 5 and 35 °C, which includes the pretransition (T_p) at 11 °C and the main acyl chain crystallization transition (T_c) at 24 °C. The projected area is shown normalized by the geometric area of the vesicle measured in a planar crystalline state (formed by moderate membrane tension) at 22 °C. Because of limitations imposed by excess area requirements and pipet to vesicle size ratio, the curves in Figure 2 are representative results from many vesicle tests; our measurements have shown that vesicle projected areas continue and overlap from one temperature range to another. The variation in this projected area ratio (A/A_o) from vesicle to vesicle is estimated to be no more than 0.005. The lower curve in Figure 2 is the projected area ratio measured at constant, low membrane tension below T_c. The intermediate curve is the projected area ratio measured at constant, moderate to high membrane tension below T_c. The upper curve is the projected area ratio measured in

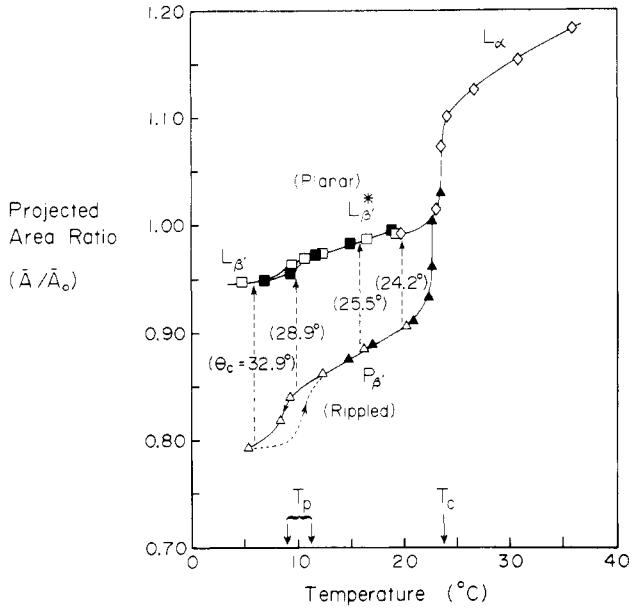

FIGURE 2: Projected area ratio versus temperature for giant DMPC vesicles in water. Heating (filled symbols) and cooling (open symbols) cycles are indicated by arrows and by the different symbols, which also refer to membrane tensions: ◇, 0.2 dyn/cm; □, 2.0 dyn/cm; ■, 2.0 dyn/cm; △, 0.6 dyn/cm; ▲, 0.16 dyn/cm.

the liquid state above T_c. (The open symbols are for decreasing temperature and the closed symbols are for increasing temperatures, respectively.) Resolution of vesicle area changes was limited by optical discrimination to the order of 0.1%.

On the basis of observed changes in vesicle area when heated and cooled through the main transition and below T_c, we found that formation of submicroscopic ripples (evidenced by reduction in apparent membrane area) depended on membrane tension. It was observed that cooling vesicles from the liquid L_α state through the main transition under zero or very low membrane tension produced area changes of about 22%. Further cooling of the vesicles to lower temperatures produced a linear decrease in the projected area followed by a second precipitous drop (about 4% change in area) in the vicinity of the pretransition. Cooling rates were kept sufficiently low so that no perceptible change in vesicle area could be detected over time at a fixed temperature. Subsequent reheating of these vesicles from 5 °C followed the same characteristic area versus temperature relation with the exception of a 3 °C hysteresis about the pretransition T_p. For temperatures below 23 °C, the vesicles could be ejected from the pipet as frozen replicas of the aspirated geometry. Reaspiration and an increase in temperature resulted in the major area expansion associated with the main transition to the liquid L_α phase. The midpoint of the main transition was 23.7 °C, and no hysteresis was detectable for the main transition even at high temperature scan rates of 10 °C/min.

Following a similar test sequence, vesicles were cooled through the main transition under moderate membrane tension of 0.2 dyn/cm; here, the area was observed to decrease only by about 12%. Application of a high membrane stress (about 2 dyn/cm) produced a very small area increase (1%) which was recoverable after the stress was removed. Reduction of the temperature to values below the pretransition produced a linear decrease in vesicle area plus a small drop at the pretransition. Subsequent reheating of the vesicle followed the same characteristic area versus temperature relation except for the small hysteresis in the vicinity of the pretransition. *Exactly* the same area versus temperature behavior was obtained for vesicles that had been annealed at 4 °C for several days, which is known to ensure the formation of the $L_{\beta'}$ phase (Ruppel & Sackmann, 1983).

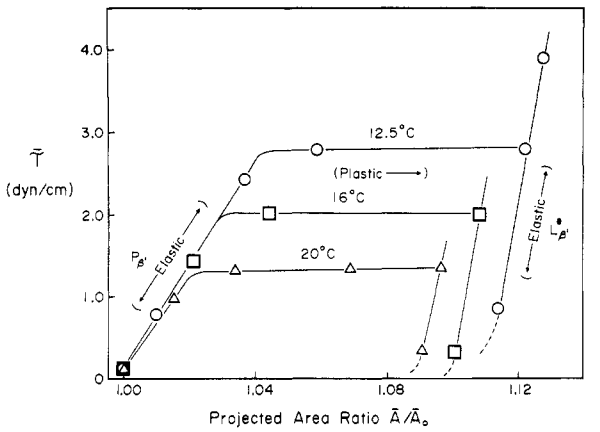

FIGURE 3: Ripple phase elasticity, yield, and plastic deformation followed by planar phase elasticity for a single vesicle. The symbols refer to three different temperatures: △, 20 °C; □, 16 °C; ○, 12.5 °C.

The final set of experiments involved application of membrane stress (tension) to vesicles held at specific temperatures below the main transition. These vesicles were initially formed in the stress-free state. Figure 3 shows the relationship between membrane tension and projected area ratio at constant temperatures of 20, 16, and 12.5 °C. In all cases, three regimes of material behavior were observed: an initial soft-elastic proportionality between tension and projected area that was essentially reversible was observed; when a threshold level of tension was reached, the surface area expanded by plastic (irreversible) deformation until it reached a limiting area; after plastic expansion to the area limit, the membrane again exhibited elastic (reversible) proportionality between membrane tension and projected area ratio but with a significantly increased stiffness. Removal of stress at this point left the vesicle in a rigid conformation with no extensional recovery of the aspirated tongue. The observed increases in projected area under plastic deformation identically matched the difference between the projected area curves shown in Figure 2 below T_c.

Hence, it was possible to produce a planar crystalline surface. This assumption is based on correlation with fractional area changes from X-ray (Janiak et al., 1979) and the measured compressibility. Three different procedures gave this planar structure: annealing at 4 °C for several days, cooling through the main transition under moderate to high stress, and plastic deformation by mechanical stress of vesicles frozen initially in the stress-free state. Since the projected area changes measured in these experiments are consistent with those deduced from X-ray diffraction studies (Janiak et al., 1979), we conclude that the initial stress-free crystallization of the vesicle bilayer results in a rippled surface superlattice. Because of the fortuitous ability to create a planar crystalline structure at temperatures intermediate between the pretransition and main transition, it was possible to directly measure the thermal area expansivity and elastic area compressibility of the lipid bilayer independent of the extrinsic superlattice. As such, the degree of lipid condensation and cohesion could be examined as a function of temperature all the way from the liquid L_α state to the low-temperature liquid crystalline $L_{\beta'}$ state. Figure 4 shows the elastic area compressibility moduli derived from measurements of tension versus fractional area expansion at fixed temperatures. A major uncertainty in this type of experiment is the number of bilayers that make

Table I: Thermoelastic Properties of Liquid and Gel Phases of DMPC in Water

phase	thermal area expansivity, C_T[a] [$(1/A)(dA/dT) \times 10^3$] ($°C^{-1}$)	elastic area compressibility modulus, K[a] (dyn/cm)	temp, T[a] (°C)
L_α	4.2 ± 0.20 (13)[b]		34.0
	6.8 ± 1.00 (25)	144.9 ± 10.5 (17)	29.0
$L^*_{\beta'}$		228.2 ± 35.0 (62)	20.0 ± 0.3
		274.2 ± 34.5 (10)	16.1 ± 0.2
	3.5 ± 0.40[c] (43)		16.0
		238.8 ± 24.4 (2)	19.6
		274.5 ± 31.0 (5)	16.7 ± 0.22
		315.8 ± 24.6 (6)	14.9 ± 0.4
	3.4 ± 0.29[d] (13)		16.0
		318.8 (1)	14.5
$P_{\beta'}$		58.7 ± 8.6 (26)	20.0
	5.8 ± 0.42 (20)	61.9 ± 0.8 (3)	16.0
		65.8 ± 2.8 (3)	12.5
$L_{\beta'}$	3×10^{-3}		8.0
		855.3 ± 140.1 (3)	8.3 ± 0.8

[a] Values C_T, K, and T are mean ± SD where appropriate. [b] Number of vesicles tested is in parentheses. [c] Ripples pulled flat or not allowed to form. [d] Ripples annealed out below T_p.

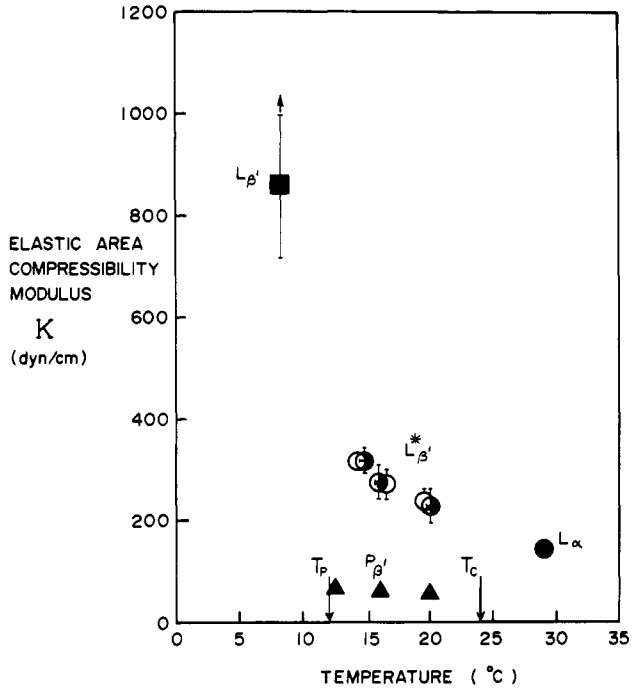

FIGURE 4: Elastic area compressibility modulus versus temperature: ●, L_α; ◑, $L^*_{\beta'}$ (ripples pulled out); ○, $L^*_{\beta'}$ (ripples annealed out below T_p); ♦, $P_{\beta'}$ before yield; ■, $L_{\beta'}$.

up the total vesicle membrane thickness. By selection of the most optically transparent vesicles (with interference contrast microscopy) and evaluation of the membrane elastic modulus, it is possible to discriminate between one, two, and more layers since the elastic modulus groups around discrete values where the lowest value is characteristic of a single bilayer (Kwok & Evans, 1981). Thus, we are confident that these measurements truly represent single-bilayer structures. Similarly, Table I presents thermal area expansivities derived from measurements of vesicle area versus temperature at constant membrane tension for the three phase domains. Even though the vesicle surfaces were rigid solids below 23 °C as demonstrated by expulsion from the micropipet, the bilayer surface compressibility was much greater at temperatures characteristic of the state of the $P_{\beta'}$ phase than at low temperatures in the $L_{\beta'}$ phase. In another paper (Evans & Needham, 1987; Needham and Evans, unpublished results), we present results from studies of membrane surface shear rigidity and viscosity (measured on vesicles over a temperature range of 5–23 °C) which are consistent with the compressibility results shown in Figure 4.

Analysis

For fixed vesicle volume, vesicle area (A) is given by a simple function of the aspiration length (L) inside the pipet, the pipet radius (R_p), and the radius of the outer spherical segment of the vesicle (R_o). Changes in total membrane area are derived from this function as

$$\Delta A = 2\pi R_p(1 - R_p/R_o)\Delta L$$

Similarly, the membrane tension T_m is given by another function of geometry times the pipet suction pressure P:

$$T_m = PR_p/(2 - 2R_p/R_o)$$

These relations were used to calculate membrane tension and area changes from the measurements of suction pressure, aspiration length, and temperature. At fixed tension, observation of the continuous change in area versus temperature within a specific lipid phase (e.g., L_α, $L_{\beta'}$, and $P_{\beta'}$) gave the thermal area expansivity:

$$C_T = \frac{1}{A_o}\left(\frac{\partial A}{\partial T}\right)$$

At fixed temperature, observation of *reversible* changes in area versus membrane tension gave the isothermal area compressibility, which is the reciprocal of the elastic area compressibility modulus:

$$K = A_o(\Delta T_m/\Delta A)$$

These two parameters completely characterize the differential equation of state for the surface when it is a plane structure (Evans & Waugh, 1977; Kwok & Evans, 1981). However, when the surface is not plane (e.g., rippled), measurements of these parameters represent expansivity and compressibility of the projected area that depend on both the extrinsic surface topography and the intrinsic molecular thermodynamics.

In order to evaluate the extrinsic effect of the superlattice, we must postulate a geometric model for the ripple structure. Based on SEM observations of freeze–fractured vesicle preparations (Luna & McConnell, 1977; Sackmann, 1983; Ruppel & Sackmann, 1983) and the simple requirement that the intrinsic crystal angle relative to the plane of a microcrystalline domain be uniform, the superlattice was modeled by the "pleated" surface illustrated in Figure 5. In general, this architecture depends on two characteristic angles: θ_c, the intrinsic crystal angle between the acyl chains and the normal to the local crystal plane, and θ_e, the extrinsic angle between the acyl chains and the normal to the *projected* plane of the superlattice. We observed that giant vesicles were made ex-

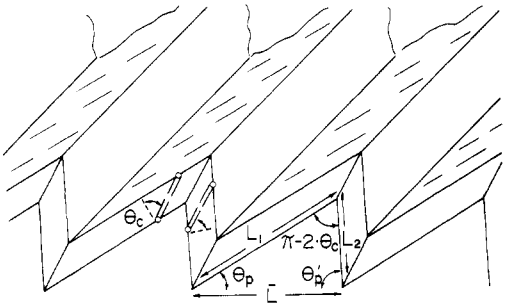

FIGURE 5: Uniformly pleated bilayer: model for $P_{\beta'}$ phase.

actly spherical with *very* low aspiration pressures even when the membranes were frozen; hence, it was apparent that the surface was made up of a great number of very small microcrystalline domains or "patches". Because of the random orientation of these "patches", differential changes in projected *area* can be derived from simple geometric analysis of the pleated phase model; i.e., the area of the pleated phase is given by

$$\bar{A} = N\tilde{A}_c[x \cos \theta_p + (1 - x) \cos \theta_p']/\cos \theta_c$$

The dependence on extrinsic angle, θ_e, has been transformed into a symmetry parameter, x, which represents a ratio of crystal pleat dimensions, i.e., $L_1/(L_1 + L_2)$, as shown in Figure 5. Also, the included angles, θ_p and θ_p', are given by

$$\theta_p = \theta_c - \theta_e$$

$$\theta_p' = \theta_c + \theta_e$$

The projected area is $\bar{A}$, and the intrinsic cross-sectional area per lipid acyl chain cylinder is $\tilde{A}_c$. N is the number of chains in the layer. Clearly, changes in projected membrane area can be produced by changes in length of the acyl chains (i.e., cross-sectional area of the molecule), in intrinsic angle of the acyl chains relative to the local bilayer normal, and in extrinsic angle between the chains and the normal to the projected plane; i.e.

$$\frac{\delta\bar{A}}{\bar{A}} = \frac{1}{\bar{A}}\left(\frac{\partial\bar{A}}{\partial\tilde{A}_c}\right)\delta\tilde{A}_c + \frac{1}{\bar{A}}\left(\frac{\partial\bar{A}}{\partial\theta_c}\right)\delta\theta_c + \frac{1}{\bar{A}}\left(\frac{\partial\bar{A}}{\partial x}\right)\delta x$$

Although the evidence is not consistent from laboratory to laboratory, results from X-ray diffraction studies indicate that the extrinsic angle, θ_e, is close to zero for the $P_{\beta'}$ phase (i.e., the acyl chains line up parallel to the normal to the projected plane) (Stamatoff et al., 1982). In order to analyze changes in projected area, it is necessary to specify the extrinsic angle, θ_e; this angle obviously becomes the intrinsic crystal angle only when the surface is a flat plane. We will assume that the extrinsic angle, θ_e, is small for the rippled surface structure in the $P_{\beta'}$ phase domain. Thus, differential changes in projected area can be calculated from either

$$\delta\bar{A}/\bar{A} = \delta\tilde{A}_c/\tilde{A}_c$$

for the rippled $P_{\beta'}$ phase, where $\theta_p \cong \theta_p' \cong \theta_c$, or

$$\delta\bar{A}/\bar{A} = \delta\tilde{A}_c/\tilde{A}_c + \tan \theta_c\, \delta\theta_c$$

for the planar $L_{\beta'}$ phase, where $x = 1.0$ and $\theta_p = 0$.

For the assumption that the acyl chains line up nearly parallel to the projected plane normal, the change in projected area at the main transition from the planar L_α liquid phase to the rippled $P_{\beta'}$ structure exactly equals the condensation of the acyl chains. From Figure 2, we see that the chain condensation is about 20%. Further, the mechanical stress induced transition at constant temperature from the rippled $P_{\beta'}$

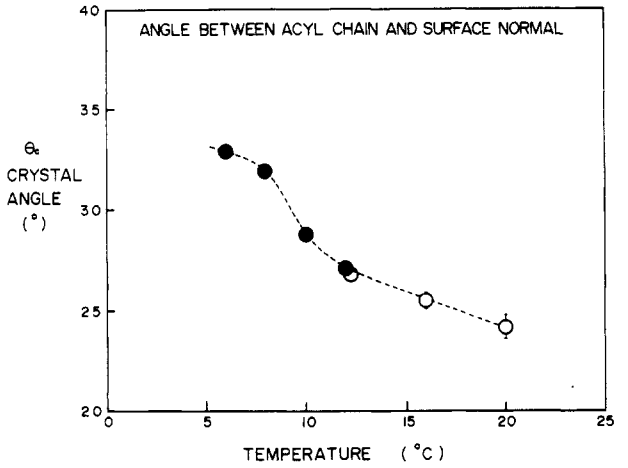

FIGURE 6: Angle between acyl chain and surface normal θ_c (crystal angle) versus temperature. ●, taken from area versus temperature plots (Figure 1) using difference between upper and lower expansivities; ○, taken directly from area change (at 2 dyn/cm) on pulling ripples flat (Figure 3).

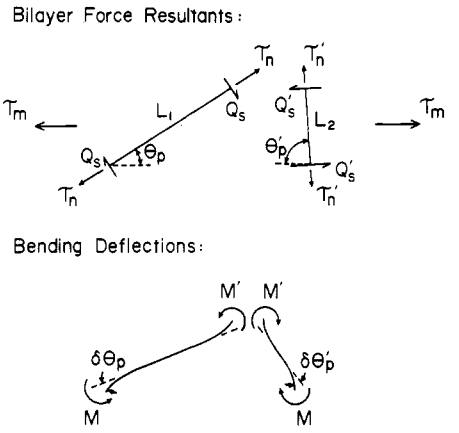

FIGURE 7: Bilayer surface force and moment resultants and bending deflections.

structure to the planar $L^*_{\beta'}$ bilayer produces changes in projected area determined by the intrinsic crystal angle, θ_c; i.e., $\Delta\bar{A}/\bar{A} = 1/\cos \theta_c - 1$. Hence, we have derived the crystal angle from the difference between the two curves shown for projected area versus temperature in Figure 2 for the crystalline phases below the main transition. Figure 6 shows the dependence of the intrinsic crystal angle on temperature.

Another major feature of the thermomechanical behavior of DMPC in the rippled $P_{\beta'}$ phase was the soft-elastic response to low membrane stress levels observed prior to plastic extension to a planar $L^*_{\beta'}$ structure (shown in Figure 3). To analyze this elastic-like response of the rippled surface, we have developed a model for the pleated phase architecture, which is illustrated in Figure 7. Briefly, the model is based on the superposition of elastic bilayer bending deflections (analogous to a corrugated spring) and surface area dilation (i.e., the small expansion in area per molecule due to the intrinsic bilayer compressibility). For a "repeat unit" of the pleated structure, Figure 7 shows a schematic illustration of the bilayer surface force and moment resultants plus the bending deflections. The force resultant, T_m, is the projected membrane tension which balances the vesicle internal pressure and in turn is composed of contributions from the bilayer crystal tension T_n and the transverse shear Q_t (Evans & Skalak, 1980). The bilayer crystal bending moment resultant M acts to bend the bilayer as shown in proportion to the change in curvature. The bending or curvature elastic relation is given by

$$M = B\Delta C$$

where B is the intrinsic bending or curvature elastic modulus of the bilayer crystal (erg) and C is the principle curvature (cm^{-1}). The continuum requirement for balance of moments along the bilayer relates the transverse shear to the tangential derivative of the bending moment (Evans & Skalak, 1980). These relations combine to give the proportionality between bending deflections ($\delta\theta_p$, $\delta\theta_p'$) and the transverse shear resultants; e.g., the deflection for one pleat of a repeat unit is

$$\delta\theta_p \cong -(Q_t/B)(L_1^2/8)$$

From force equilibrium, the transverse shear in the pleat is related to the projected membrane tension by

$$Q_t = T_m \sin\theta_p$$

Finally, simple geometry shows that the projected extension of the repeat unit $\delta\bar{L}$ is given by the bending deflection times the peak-to-peak amplitude a of the ripple:

$$\delta\bar{L} = -a(\delta\theta_p + \delta\theta_p')$$

Hence, we arrive at the elastic "constitutive" relation for the pleated surface as an incompressible structure:

$$T_m = \mu_B(\delta\bar{L}/\bar{L})$$

where μ_B is the effective extensional modulus and is given by

$$\mu_B = (8B/a^2)[x\cos\theta_p + (1-x)\cos\theta_p']$$

For the assumption that the acyl chains line up parallel to the projected plane normal, the extensional modulus is simply proportional to the bending stiffness divided by the square of the ripple amplitude:

$$\mu_B = (8B/a^2)\cos\theta_c$$

The mechanical "advantage" of the pleated surface is immediately evident because the extensional rigidity is inversely proportional to the square of the ripple amplitude. Again, since the surface appears to be made up of a large number of small randomly oriented microcrystalline domains, we can simply transform the extensional constitutive relation for the repeat unit into an elastic relation for surface area expansion and include the additional effect of the planar bilayer compressibility; i.e.

$$\frac{\delta\bar{A}}{A} \cong T_m\left(\frac{1}{\mu_B} + \frac{1}{K}\right)$$

Discussion and Conclusions

The primary deduction from this work is that the presence of submicroscopic ripples (which characterize the $P_{\beta'}$ gel phase of saturated lecithins) depends on stress history; i.e., for zero to low membrane stresses the surface ripple can form. Above moderate stress levels a metastable planar phase is formed, termed $L^*_{\beta'}$, which exists over the same temperature range between T_c and T_p. Measurement of bilayer compressibility in the gel phase domain clearly demonstrates that the $P_{\beta'}$ phase is indeed much more compressible (liquidlike) than the $L_{\beta'}$ phase, which directly confirms many of the conclusions derived from the spectroscopic data discussed previously. Furthermore, the formation of the $P_{\beta'}$ superlattice is not the origin of the enthalpy change at the pretransition.

Specific conclusions were derived from four types of experiments which describe this stress history and the formation of the metastable $L^*_{\beta'}$ phase:

(i) Vesicles were cooled from the L_α phase through T_c under zero or very low membrane tension (0.2 dyn/cm). Here, the $P_{\beta'}$ phase formed with a ripple superlattice. We assume that the lipid molecules were oriented close to the perpendicular to the projected plane and remained so with decreasing temperature. Hence, the observed vesicle area change for the whole lower line in Figure 2 represents area condensation per molecule. It has been reported from SEM studies that it takes hours to days to fully anneal out the rippled structure (Ruppel & Sackmann, 1983). The ripple reduces to steps to produce the planar $L_{\beta'}$ phase. In the time of our experiments (minutes to 1 h) there appeared to be no annealing out of ripples upon cycling through the pretransition, in agreement with the SEM observations. Thus, the area change at the pretransition indicated a fairly rapid conformational rearrangement (approximately minutes), and the $P_{\beta'}$ ripple structure itself did not relax to the planar $L_{\beta'}$ phase. We were therefore able to cool below T_p with the ripple structure kinetically trapped. Hence, area changes in the low-temperature region also represent changes in area per molecule.

It is interesting to note that the changes in relative area per molecule at T_c and T_p of 22% and 4% are in a similar ratio to the respective excess specific heats reported from DSC measurements (Lentz et al., 1978; Mabrey & Sturtevant, 1976), i.e., 5–6:1. Furthermore, the excess specific heat does not go to zero between T_c and T_p, and the excess enthalpy changes in much the same way as vesicle area (Hinz & Sturtevant, 1972). The ~3 °C hysteresis that we observed at the pretransition has also been found in DSC and spectroscopic studies (Lentz et al., 1978; Luna & McConnell, 1977).

In the L_α phase, the decreasing thermal area expansivity with increasing temperature is consistent with an approach to gauche–kink saturation and to a thermal expansivity similar to natural egg lecithin (Kwok & Evans, 1981) at temperatures well above the the bilayer gel to liquid phase transition. Although the thermal expansivity at temperatures below T_p could not be measured with the same accuracy as in the $P_{\beta'}$ phase, due to the limited range of temperature and hysteresis effects, it still appeared to be significant ($\sim 3 \times 10^{-3}$/°C).

(ii) Vesicles were subjected to moderate stress levels (~0.5 dyn/cm) by applied pipet suction and cooled from the L_α phase through T_c. Here, reduced area changes were observed for the main transition (upper line below T_c in Figure 2). Under these conditions the ripple phase was prevented from forming and a metastable phase was produced, which we have termed $L^*_{\beta'}$. On the basis of the area change, we assume it to be planar crystalline, with acyl chains tilted to the bilayer normal, as in the low-temperature $L_{\beta'}$ phase. If the membrane tension was reduced to zero immediately following the main transition, a small additional area reduction was observed, indicating partial ripple formation. Hence, some molecular relaxation was necessary to attain a stationary $L^*_{\beta'}$ phase and was achieved by holding the vesicle in the newly frozen state under moderate tension for an extended period of time.

The area change from L_α to $L^*_{\beta'}$ was 11–12%, in agreement with the value obtained previously by Evans and Kwok (1982). In their experiment the measurement of compliance at T_c necessitated cooling through the transition under moderate to high stress levels (0.3–1.7 dyn/cm), and it is clear from the present observations that the vesicles entered the $L^{*\beta'}$ phase. Hence, their conclusion that the transition, on the basis of the observed area change, was between L_α and an $L^*_{\beta'}$ phase is confirmed by the present study.

(iii) Vesicles with sufficient excess area to pass through the main transition unstressed and so form the $P_{\beta'}$ phase were refrigerated at 4 °C for several days to allow annealing to the

$L_{\beta'}$ phase. Pipet aspiration at low temperature to produce high tension (~6 dyn/cm) caused very little inelastic area change, which indicated an absence of ripples. The small amount of area increase after stress was most likely due to macroscopic smoothing of the surface. When the vesicles were heated, the projected area followed the upper curve of Figure 2 to the L_α phase, and so, transitions between the three planar phases were observed, $L_{\beta'} - L^*_{\beta'} - L_\alpha$.

(iv) Finally, vesicles were subjected to high membrane tensions (0–3 dyn/cm) at three temperatures between T_c and T_p which had been performed in the rippled phase by cooling from the L_α phase under zero tension. The initial response to low tensions was elastic (Figure 3). The subsequent permanent dilation of projected area represented plastic extension and elimination of the ripple superlattice. Hence, in this experiment we measured the ripple elasticity, the yield tension for ripple elimination, the total area change from the ripple to planar sheet, and the compressibility of the planar $L^*_{\beta'}$ phase. The process provided a temperature-independent pathway to go from the lower to intermediate lines on Figure 2.

With the only assumption that the lipid molecules are nearly perpendicular to the projected plane, a view supported by X-ray (Stamatoff et al., 1982), the difference in projected area between the $P_{\beta'}$ and the $L^*_{\beta'}$ phases gives the crystal angle, θ_c, directly; i.e.

$$(\text{area rippled}/\text{area planar}) = \cos \theta_c$$

As shown in Figure 2 and plotted in Figure 6, the intrinsic crystal angle calculated by this method increased from 24° to 29° over the $P_{\beta'}$ temperature region and increases to ~33° below the pretransition. As mentioned earlier, it is possible to obtain these angle estimates from area differences even below the pretransition because the secondary ripple structure was kinetically trapped on the time scale of the experiment. θ_c values determined directly from elimination of ripples and, graphically, from area versus temperature plots at high and low stress are shown to be in excellent agreement. The θ_c values that we calculated for the $P_{\beta'}$ phase are slightly lower than those derived from earlier X-ray studies (Janiak et al., 1976) where a constant value of 30° was estimated by comparing the bilayer thickness of 44.5 Å with that calculated for DMPC with fully extended chains oriented normal to the bilayer plane. Since it appears that the $P_{\beta'}$ phase possesses some degree of rotameric disorder, a less than fully extended chain assumption would be more appropriate. Thus, using the X-ray bilayer thickness value of 44.5 Å and our increasing crystal angles from 24° to 29°, we calculate an increase in twice the DMPC chain length from 48.7 to 50.9 Å between T_c and T_p. Compare this with twice the estimated fully extended chain length for DMPC of 51.6 Å (Janiak et al., 1976), and the two sets of data indicate that the $P_{\beta'}$ phase must possess some degree of disorder. If the ripple structure was slightly asymmetric (as shown in Figure 3), our results would be little affected.

It is clear from the above that molecular condensation in the gel phases of DMPC occurs by virtue of the lipid molecules being able to increase their angle of tilt to the bilayer normal. At the pretransition, further condensation forces a larger change in tilt angle and the ripple structure becomes unstable and reverts to a planar configuration. However the secondary ripple itself is a metastable consequence of molecular packing and can be converted to a planar arrangement at constant crystal angle by the application of membrane stress. The work required to do this (tension × area change) is some 50 times less than the enthalpy associated with the pretransition (Lentz et al., 1978; Mabrey & Sturtevant, 1976). Thus, the plastic deformation does not significantly alter chain configurations that are established by the pretransition. It is likely that melting and refreezing of lipid occurs at the peaks and troughs as the ripple is pulled flat. The yield tension is in fact seen to increase with decreasing temperature, indicating a greater mechanical energy required for such localized melting the further one gets from the melting transition.

Examination of the soft-elastic response shown in Figure 3 yields values for the effective compressibility modulus of about 60 dyn/cm. As noted in the introduction, X-ray diffraction studies indicate that the peak-to-peak amplitude of the surface ripples is about 50–80 Å for DMPC. With values for ripple amplitude and the elastic compressibility modulus measured for the planar crystal bilayer (shown in Figure 4), we can determine the bending or curvature elastic modulus of the planar $L^*_{\beta'}$ crystal bilayer; i.e., $B \sim 3 \times 10^{-12}$ erg. Based on a simple elastic theory for bending of coupled molecular layers (Evans & Skalak, 1980), the calculated bending stiffness agrees very well with the theoretical prediction if we use the measured area compressibility modulus of the crystal bilayer and published values for bilayer thickness. As expected, the bending modulus is larger than measured values for lipid bilayers in the L_α state (Servuss et al., 1978; Schneider et al., 1984) in proportion to the area compressibility modulus.

Elastic compressibility measurements on the planar phases L_α, $L^*_{\beta'}$, and $L_{\beta'}$ (Figure 4) also clearly show that the bilayer between T_c and T_p possesses some liquid character even though the lipid has undergone a major acyl chain freezing transition. The elastic area compressibility modulus in the $L^*_{\beta'}$ phase is only a factor of 2–3 times higher than that in the liquid L_α phase. The modulus increases with decreasing temperature, and below the transition further condensation produces a much less compressible $L_{\beta'}$ phase as shown by the severalfold increase in K.

The stress history behavior described here should be observable by other techniques, especially SEM. Such studies have not reported an absence of ripple, being more concerned with the ripple itself, although some vesicles in a typical preparation do show varying ripple wavelength, and some have smooth surfaces (E. Sackmann, personal communication). It is expected and found in the present work that a typical vesicle preparation can have a heterogeneity in vesicle area/volume ratio such that three events may occur, depending on the buildup or absence of thermoelastic stress in the vesicle membrane upon cooling through the main transition. At large area/volume ratios the vesicles may undergo the large (22%) area change without sphering and form the $P_{\beta'}$ phase in the stress-free state. At small area/volume ratios the vesicles sphere during the transition and rapidly build up thermoelastic stress, causing rupture. These may also partially form $P_{\beta'}$ phase when the thermoelastic stress is released (the hole in the membrane is only sealed by reheating). At intermediate ratios some vesicles may just make it through the transition and form spheres with varying amounts of membrane tension (up to 5 dyn/cm). Since, as the present experiments have shown, very low levels of tension are required to prevent the ripple from forming (0.5 dyn/cm), this group of vesicles would have rippled structure to a greater or lesser extent depending on the level of thermoelastic stress that developed. Thus, the application of pipet suction to spherical vesicles below T_c was found to give varying amounts of area change up to the maximum shown in Figure 3, indicating such a heterogeneity in ripple content. It might be interesting to osmotically adjust the area/volume ratio of a homogeneous size preparation of

single-walled vesicles such that a thermoelastic stress builds up as indicated above and examine the vesicle population by SEM. Hence an attempt may be made to correlate absence of ripple and the reported range of ripple wavelengths with the thermoelastic stress in the membrane.

Registry No. DMPC, 13699-48-4.

REFERENCES

Brady, G. W., & Fein, D. B. (1977) *Biochim. Biophys. Acta 464*, 249–259.

Büldt, G., Seelig, A., & Seelig (1979a) *J. Mol. Biol. 134*, 693–706.

Büldt, G., Galley, H. U., & Seelig, J. (1979b) *J. Mol. Biol. 134*, 673–691.

Cameron, D. S., Casal, H. L., & Mantsch, H. H. (1980) *Biochemistry 19*, 3665–3672.

Casal, H. L., & Mantsch, H. H. (1984) *Biochim. Biophys. Acta 779*, 381–401.

Chapman, D., Williams, R. M., & Ladbrooke, B. D. (1967) *Chem. Phys. Lipids 1*, 445–475.

Chen, S. C., Sturtevant, J. M., & Gaffney, G. J. (1980) *Proc. Natl. Acad. Sci. U.S.A. 77*, 5060–5063.

Cullis, P. R. (1976) *FEBS Lett. 70*, 223–228.

Davis, J. H. (1979) *Biophys. J. 27*, 339–358.

Davis, J. H. (1983) *Biochim. Biophys. Acta 737*, 117–171.

Evans, E. A., & Waugh, R. (1977) *J. Colloid Interface Sci. 60*, 286–298.

Evans, E. A., & Skalak, R. (1980) *Mechanics and Thermodynamics of Biomembranes*, CRC Press, Boca Raton, FL.

Evans, E. A., & Kwok, R. (1982) *Biochemistry 21*, 4874–4879.

Evans, E. A., & Needham, D. (1987) in *Physics of Amphiphilic Layers* (Meunier, J., Langevin, D., & Boccara, N., Eds.) Springer-Verlag, Berlin and Heidelberg.

Hinz, H.-J., & Sturtevant, J. M. (1972) *J. Biol. Chem. 247*, 6071–6075.

Janiak, M. J., Small, D. M., & Shipley, G. G. (1976) *Biochemistry 15*, 4575–4580.

Janiak, M. J., Small, D. M., & Shipley, G. G. (1979) *J. Biol. Chem. 254*, 6068–6078.

Krebecek, R., Gebhardt, C., Gruber, H., & Sackmann, E. (1979) *Biochim. Biophys. Acta 554*, 1–22.

Kwok, R., & evans, E. A. (1981) *Biophys. J. 35*, 637–652.

Larsson, K. (1977) *Chem. Phys. Lipids 20*, 225–228.

Lentz, B. R., Friere, E., & Biltonen, R. L. (1978) *Biochemistry 17*, 4475–4480.

Levin, I. W., & Bush, S. F. (1981) *Biochim. Biophys. Acta 640*, 760–766.

Luna, E. J., & McConnell, H. M. (1977) *Biochim. Biophys. Acta 466*, 381–392.

Luzzati, V., & Husson, F. (1962) *J. Cell Biol. 12*, 207–219.

Mabrey, S., & Sturtevant, J. M. (1976) *Proc. Natl. Acad. Sci. U.S.A. 73*, 3862–3866.

MacKay, A. L. (1981) *Biophys. J. 35*, 301–313.

Marsh, D. (1980) *Biochemistry 19*, 1632–1637.

Mueller, P., Chien, T. F., & Rudy, B. (1983) *Biophys. J. 44*, 375–381.

Nagle, J. F. (1980) *Annu. Rev. Phys. Chem. 31*, 157–195.

Pink, D. A., Green, T. J., & Chapman, D. (1980) *Biochemistry 19*, 349–356.

Rand, R. P., Chapman, D., & Larsson, K. (1975) *Biophys. J. 15*, 1117–1124.

Reeves, J. P., & Dowben, R. M. (1969) *J. Cell Biol. 73*, 49–60.

Ruocco, M. J., & Shipley, G. G. (1982) *Biochim. Biophys. Acta 691*, 309–320.

Rüppel, D., & Sackmann, E. (1983) *J. Phys. (Les Ulis, Fr.) 44*, 1025–1034.

Sackmann, E. (1983) *Biophysics* (Hoppe, W., Lohmann, W., Markl, H., & Ziegler, H., Eds.) Springer-Verlag, Berlin and Heidlberg.

Schneider, M. B., Jenkins, J. T., & Webb, W. W. (1984) *J. Phys. (Les Ulis, Fr.) 5*, 1457.

Servuss, R. M., Harbich, W., & Helfrich, W. (1978) *Biochem. Biophys. Acta 436*, 900–903.

Snyder, R. G., Cameron, D. G., Casal, H. L., Compton, D. A. C., & Mantsch, H. H. (1982) *Biochim. Biophys. Acta 684*, 111–116.

Stamatoff, J., Fever, B., Guggenheim, H. J., Tellez, G., & Yamene, T. (1982) *Biophys. J. 38*, 217–226.

Tardieu, A., Luzzati, V., & Reman, F. C. (1973) *J. Mol. Biol. 75*, 711–733.

Vogel, H., & Jähnig, F. (1981) *Chem. Phys. Lipids 29*, 83–101.

Wong, P. T. T. (1984) *Annu. Rev. Biophys. Bioeng. 13*, 1–24.